bnhcrc.com.au

bushfire&natural HAZARDSCRC

THE EFFECTS OF FIRE-PLUME DYNAMICS ON THE LATERAL AND LONGITUDINAL SPREAD OF LONG-RANGE SPOTTING

PROCEEDINGS OF THE RESEARCH FORUM AT THE BUSHFIRE AND NATURAL HAZARDS CRC & AFAC CONFERENCE
WELLINGTON, 2 SEPTEMBER 2014

William Thurston[1], Kevin J. Tory[1], Jeffrey D. Kepert[1] and Robert J. B. Fawcett[1,2]
[1]Centre for Australian Weather and Climate Research
[2]The Bureau of Meteorology

Corresponding author: w.thurston@bom.gov.au

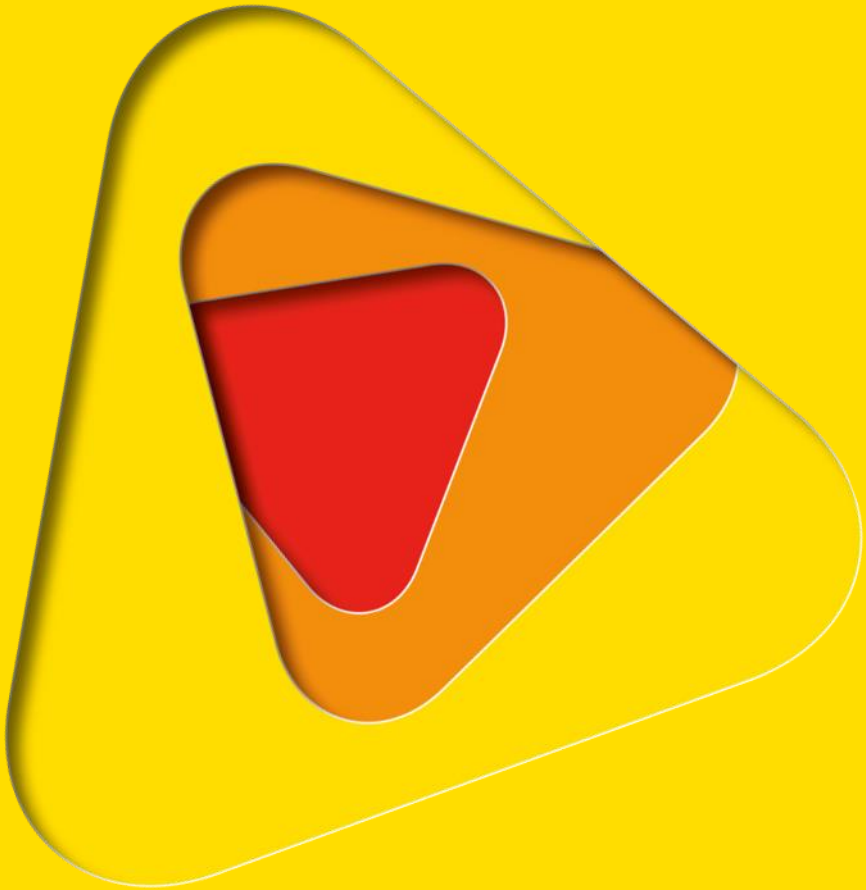

Publisher:
Bushfire and Natural Hazards CRC

January 2015

TABLE OF CONTENTS

The effects of fire-plume dynamics on the lateral and longitudinal spread of long-range spotting

William Thurston*[1,2], Kevin J. Tory[1,2], Jeffrey D. Kepert[1,2] and Robert J. B. Fawcett[1,2,3]

[1]*The Centre for Australian Weather and Climate Research, Docklands, Vic. 3008, Australia*
[2]*Bushfire and Natural Hazards CRC, Albert Street, East Melbourne, Vic. 3002, Australia*
[3]*The Bureau of Meteorology, Docklands, Vic. 3008, Australia*

Abstract

The lofting of firebrands from bushfires into a background atmospheric flow can lead to spotting downwind of the fire front. Spotting is a hazardous phenomenon because it leads to both unpredictable and accelerated fire spread, as winds aloft are often in a different direction from and faster than the near-surface winds. Here we use a two-stage modelling process to address some of the uncertainty associated with spotting, by quantifying the lateral and longitudinal spread in the landing location of potential firebrands and how this spread is affected by the dynamics of the fire plume.

Firstly, we present high resolution, three-dimensional numerical simulations of bushfire plumes using the UK Met Office Large-Eddy Model (LEM). Plumes are simulated under a range of background wind conditions and the intensity, size, morphology and temporal stability of the resulting plumes are examined. Secondly, we use a Lagrangian particle transport model to calculate the trajectories of particles released near the base of each plume. Particles are assigned fall velocities representative of common firebrands and then advected by the three-dimensional velocity fields from the LEM simulations minus the specified fall velocity. By calculating the trajectories of hundreds of thousands of potential firebrands for each plume, distributions of landing position are constructed. We find that: (i) interaction between the plume updraft and the background wind determines the distance travelled by firebrands, and (ii) the morphology of the plume determines the lateral and longitudinal spread of landing positions. These variations need to be properly accounted for in predictive models of fire spread and systematic studies such as this form the building blocks of better empirical spotting models.

1 Introduction

Fire spotting is a hazardous phenomenon which can lead to unpredictable fire behaviour and accelerated fire spread. Spot fires occur when firebrands are lofted into strong ambient winds and ignite new fires downwind; the process being called spotting. This spotting increases the unpredictability and speed of fire spread because winds aloft are often in a different direction from and faster than the near-surface winds. An idea of the magnitude of the problem is given by Cruz et al. (2012), who present evidence of long-range spotting in excess of 30 km during the Black Saturday bushfires of February 2009. A thorough knowledge of the potential for lofting from a fire is therefore desirable in order to accurately predict the rate of spread and coverage of bushfires. In this paper we attempt to address

*W.Thurston@bom.gov.au

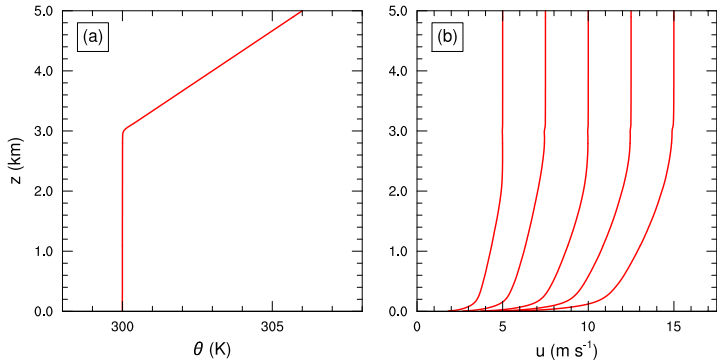

Figure 1: Domain-averaged profiles of the mean conditions in the spun-up quasi-steady state atmosphere prior to plume initialisation. (a) Potential temperature, K, and (b) horizontal wind speed, m s^{-1}, for each of the five different background-wind simulations.

some of the uncertainty associated with spotting by specifically considering how interactions between the fire plume and the atmosphere may affect (i) the distance travelled by potential firebrands and (ii) the lateral and longitudinal spread in potential-firebrand landing positions.

2 Methodology

We use a two-stage modelling approach to calculate the landing position of potential firebrands. Firstly we perform numerical simulations of idealised bushfire plumes under various wind conditions, using the UK Met Office Large-Eddy Model (LEM), Gray et al. (2001). We then use the three-dimensional velocity fields produced by the LEM to calculate the paths travelled by particles with assigned fall velocities that are released near the base of the simulated plumes.

2.1 Plume simulation

The plume simulation technique employed is fully described in Thurston et al. (2013), so we provide only a brief overview here. The plume simulations are carried out using the LEM. All plume simulations are performed in a domain of horizontal size 38.4 km by 19.2 km and a uniform horizontal grid length of 50 m. The vertical grid length increases smoothly from 10 m near the land surface to 50 m near the model top at 10 km above ground level (AGL). The plume simulations are themselves a two-stage process, which consists of firstly spinning up an appropriate base-state atmosphere in which to conduct the plume simulation and secondly simulating the plume itself.

The base-state atmosphere is spun up by initialising the model with the horizontally uniform potential-temperature profile shown in Fig. 1 (a). This profile consists of a 3.0-km deep well-mixed layer with constant potential temperature of 300 K, and a stably stratified troposphere with a gradient of 3.0 K km^{-1} above the mixed layer. The model is initialised with a horizontally and vertically uniform wind velocity throughout the domain. Small random perturbations with a maximum amplitude of ± 0.1 K are added to the initial potential temperature field below 3 km AGL to initiate turbulence within the mixed layer and the model is then run to a quasi-steady state, as determined by the domain-averaged turbulent kinetic energy (TKE).

We spin up five different base states which differ in the strength of their initialisation wind velocity, namely downwind speeds of $u = 5.0, 7.5, 10.0, 12.5$ and 15.0 m s^{-1} and crosswind speeds of $v = 0.0$ m s^{-1} for each case. The resulting wind profiles for the five different base states are shown in

Fig. 1 (b). Spinning up the turbulence has resulted in the development of a logarithmic wind profile within the mixed layer and little change to the potential-temperature profile. The 3-km deep mixed layer in the base state potential temperature profile is representative of moderately severe fire-weather conditions, but not as extreme as the 5-km deep mixed layer seen on Black Saturday (Fawcett et al., 2013), and the wind speeds represent a range from moderate to strong.

An idealised bushfire plume is simulated in each atmospheric base state by imposing a localised intense sensible heat flux anomaly at the model's lower boundary to represent the heat that the fire inputs to the atmosphere. The anomaly is constructed of a circle with a radius of 250 m, within which a uniform sensible heat flux of 1×10^5 W m^{-2} is specified. The centre of this circular heat source is located 2 km from the upwind boundary in the $x-$direction and equidistant from the lateral boundaries in the $y-$direction. A passive tracer is also emitted at a constant rate from the surface within the area of the sensible heat flux anomaly, for plume visualisation purposes. In each background-wind case the plume is well developed after 30 minutes of simulation time with the surface heat flux anomaly applied and the simulation is then continued for a further 60 minutes. During this period the three-dimensional velocity fields are saved at 5-second intervals to be used in the firebrand trajectory calculations.

2.2 Firebrand trajectory calculation

We use a very simple Lagrangian particle-transport model for calculating the trajectories of potential firebrands. This is justified as the focus of our study is to specifically investigate the effects of the plume dynamics on firebrand transport, rather than the many other factors involved, such as firebrand type, size, weight, rotation and burnout time, which are described by more complex firebrand models (e.g. Anthenien et al., 2006; Sardoy et al., 2007; Oliveira et al., 2014).

Virtual particles are initialised near the base of the plume and the three-dimensional velocity fields produced by the LEM at 5-second intervals are linearly interpolated in space and time to the position of each particle. A vertical velocity of $w = -6.0$ m s^{-1} is added to the velocity field used to advect the particles, to represent a typical fall speed for flakes of jarrah and karri bark (Ellis, 2010). The particles are then advected forward in time, using a second-order Runge-Kutta method with a 0.05 s timestep (similar to the timestep used in the LEM plume modelling) until they reach the land surface.

In the trajectory calculations presented here particles are initialised in a cylinder of radius 250 m and depth 50 m, positioned between $z = 50$ and $z = 100$ m AGL. The particles are located on a Cartesian grid with equal x, y, z-spacings of approximately 10 m between particles, leading to a total number of 8265 particles occupying the cylinder. We release 8265 particles once every 5 seconds for 15 minutes and then calculate the trajectories of the particles until all have landed on the land surface. This means that we release 1,487,700 particles for each plume simulation. Many particles fall to the ground without being lofted or travelling any appreciable distance. As we are interested in the plume-modulated long-range spotting we only consider particles that have travelled a horizontal distance of greater than 1 km when compiling statistics of landing position. This represents about 30% of the initialised particles for each plume and we denote these "launched" particles.

3 Results

3.1 Plume simulations

We concentrate our analysis of plume dynamics on the two extreme cases simulated, the 5.0 and 15.0 m s^{-1} background wind cases. Three-dimensional visualisations of the instantaneous passive-tracer field for these two cases are shown in Fig. 2. Under the weakest background winds the plume

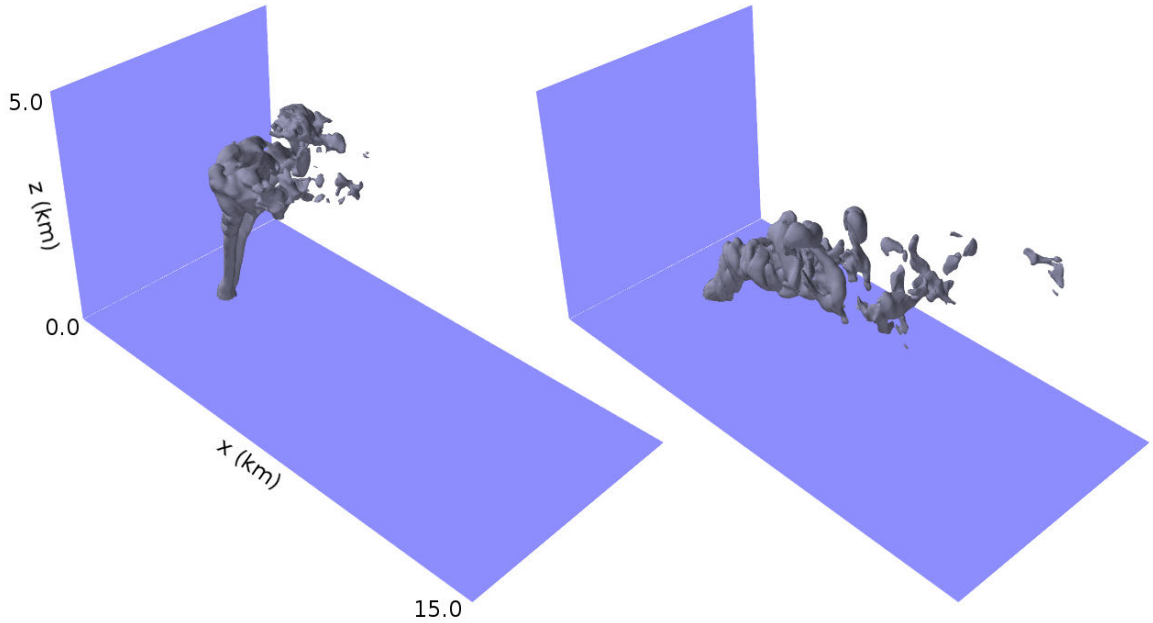

Figure 2: Snapshots of instantaneous concentration isosurface of a passive tracer released at a constant rate from the surface over the area representing the fire. The left-hand panel is the 5.0 m s^{-1} background-wind simulation and the right-hand panel is the 15.0 m s^{-1} background-wind simulation.

is almost upright. The lower half of the plume appears to be smooth and reasonably narrow, with the upper half of the plume broadening and becoming more turbulent. In comparison, the plume under the strongest background winds is much more bent over and is broader and more turbulent almost entirely throughout its vertical extent. Animations of the passive tracer field reveal that in the 5.0 m s^{-1} background wind simulation the lower half of the plume is steady, with the exception of some shear instability forming at the top of the smooth region. The lower half of the plume also appears to be bifurcating, a feature which is examined in more detail later. Animations reveal that in the 15.0 m s^{-1} background wind simulation the plume exhibits puffing and meandering behaviour.

Fig. 3 (a) shows a vertical cross-section along the plume centreline of the instantaneous vertical velocity associated with the plume in the 5.0 m s^{-1} background-wind simulation. This snapshot reveals a smooth, narrow and almost upright plume updraft which extends above the top of the mixed layer, located at 3.0 km AGL. The shear instability mentioned in Fig. 2 is visible along the leading edge of the updraft, in the form of three local updraft maxima located at heights of approximately $1.8, 2.4$ and 3.0 km AGL. The updraft is strong, with vertical velocities in excess of 25 m s^{-1} present.

In Fig. 3 (b)-(d) we present plan views at three different heights of the plume vertical velocity and anomalous horizontal velocity, where the anomaly is defined with respect to the domain-averaged horizontal velocity at the height of the plan view being displayed. At a height of 242.7 m AGL the updraft has a kidney-like shape, with a much greater vertical velocity on the upwind side of the plume and strong inflow into the back of the updraft. By 1176.8 m AGL the plume has developed into two distinct updraft cores and there is strong rotation around each of these updrafts. This is indicative of a counter-rotating vortex pair. At 2495.7 m AGL, where we are approaching the top of the mixed layer, the horizontal symmetry in the updrafts has begun to break down. We no longer see two distinct rotating updrafts of equal magnitude, but rather some asymmetric horizontal stretching of the updrafts, to the point of some coherent secondary updrafts beginning to break away, maintaining some horizontal circulation. These are weak wake vortices being shed from the main updraft plume. The presence of shear instability, wake vortices and a counter-rotating vortex pair is consistent with the descriptions and visualisations of vortices generated by strong updrafts in the pioneering work of Fric and Roshko

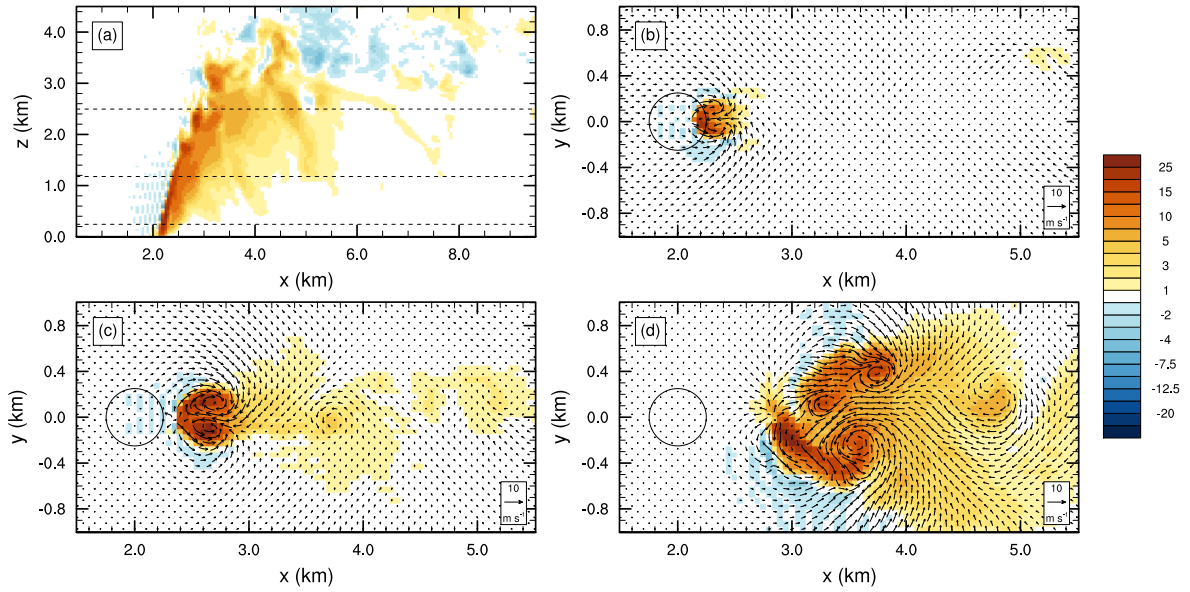

Figure 3: (a) Vertical cross-section (in the $y = 0$ plane) of the instantaneous plume updraft (solid fill, m s^{-1}) in the 5.0 m s^{-1} background-wind simulation. (b)–(d) Plan views of the instantaneous plume updraft (solid fill) and anomalous horizontal wind (curly vectors) at heights of $z = 242.7, 1176.8$ and 2495.7 m AGL. The horizontal dashed lines in (a) denote the locations of the plan views shown in (b)–(d) and the circles in (b)–(d) denote the location of the surface heat source.

(1994), in particular, the schematic in their Fig. 1.

Inspection of the corresponding vertical cross section and plan views for the plume in the 15.0 m s^{-1} background-wind plume simulation (Fig. 4) highlights the different plume dynamics. The updraft has a smaller vertical velocity, does not reach the top of the mixed layer and is much less coherent. There are many local updraft maxima visible along the upper edge of the plume in the vertical cross section, highlighting the presence of many puffs. The plan views do not reveal any large-scale coherent rotation, but do confirm the turbulent nature of this plume with a little small scale rotation also visible around the individual updraft puffs.

3.2 Firebrand trajectory simulations

In Fig. 5 we present the trajectories of 100 individual potential firebrands, chosen at random, that were launched by plumes in the 5.0 and 15.0 m s^{-1} background wind simulations. In the case of the 5.0 m s^{-1} background wind simulation, the counter-rotating vortex pair which makes up the lower section on the plume is lifting the firebrands up in two distinct, but narrowly separated columns. Once the firebrands reach the more turbulent region of the plume, this narrow separation increases and by the time the firebrands begin to fall out of the plume they have a very wide lateral spread. In contrast, the paths travelled by the potential firebrands lofted by the plume in the in the 15.0 m s^{-1} background wind simulation have very little lateral spread, but enormous longitudinal spread. This is caused by the turbulent and very puffy nature of the plume, which leads to groups, or "clumps", of particles being suspended only if they are within an updraft of sufficient strength to carry them. Not only does this lead to the large longitudinal spread, but it also leads to the potential firebrands falling out in clusters, as seen at approximately $x = 4$–6 km, $x = 9$–11 km and $x = 14$–17 km.

A more general view of the spotting characteristics of all of the particles launched by the plumes for all five background wind condition simulations is given by the two-dimensional landing position

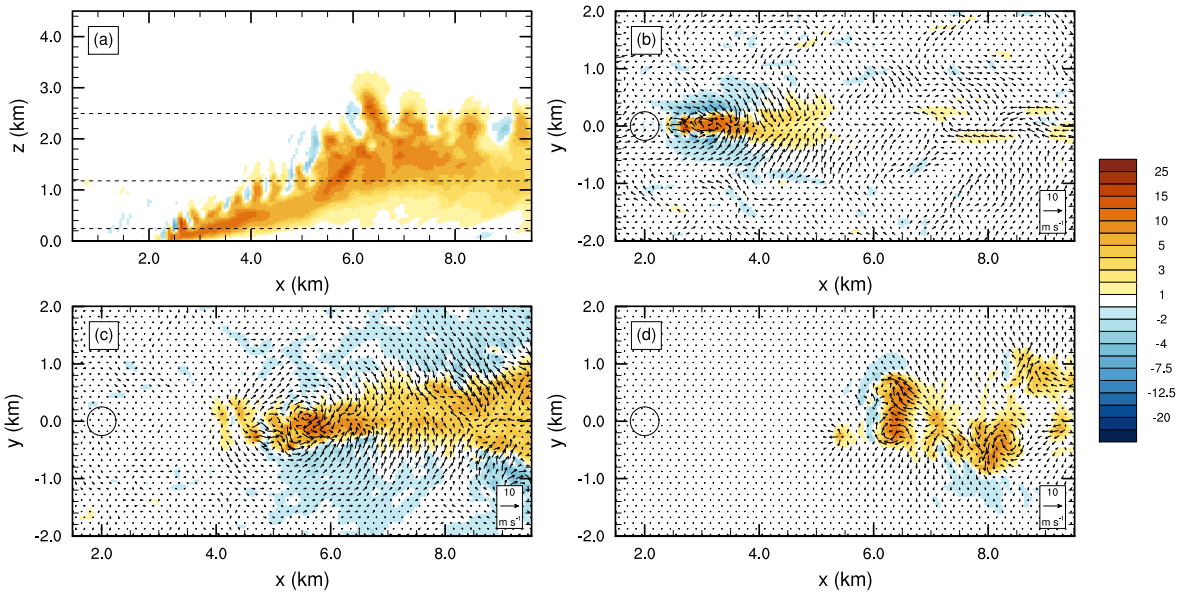

Figure 4: As in Fig. 3, but for the 15.0 m s^{-1} background-wind simulation.

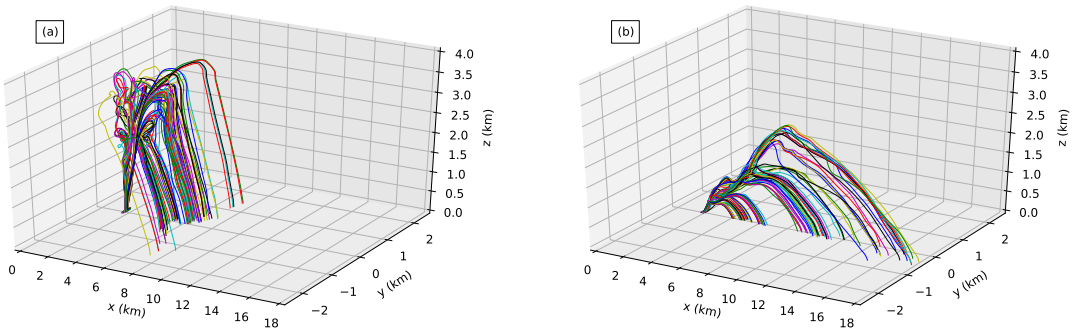

Figure 5: Three-dimensional trajectories of 100 randomly chosen potential firebrands lofted by plumes in the (a) 5.0 and (b) 15.0 m s^{-1} background-wind simulations.

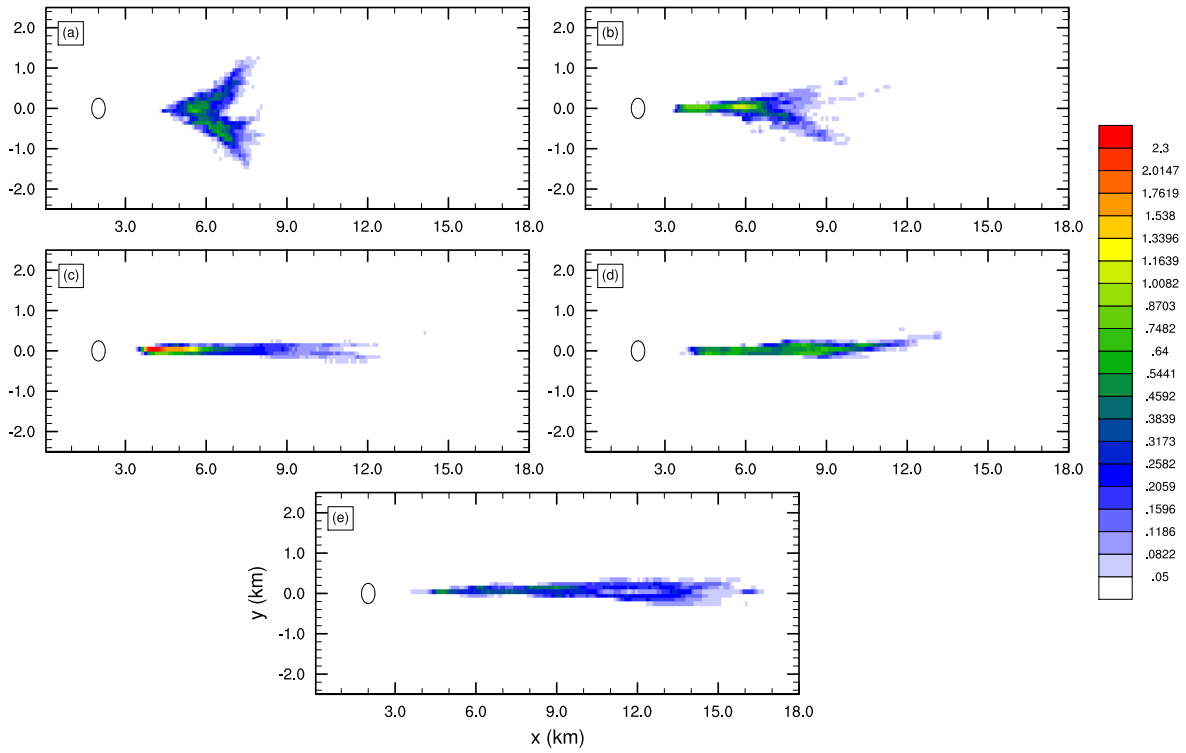

Figure 6: Two-dimensional spatial distributions of potential-firebrand landing position (solid fill, percent of particles launched per km^2) in the (a) 5.0, (b) 7.0, (c) 10.0, (d) 12.5 and (e) 15.0 m s^{-1} background-wind simulations.

distributions in Fig. 6. Under the weakest background winds, the strong lateral variability caused by the counter-rotating vortex pair has resulted in a v-shaped pattern of landing positions. As the strength of the background wind increases, three features are clear.

Firstly, the distance travelled by the potential firebrands increases. The mean (maximum) distance travelled by potential increases from 4.3 km (7.6 km) downwind of the launching position in the weakest background-wind simulation to 8.3 km (18.7 km) downwind of the launching position in the strongest background-wind simulation.

Secondly, the lateral spread of the landing positions decreases as the background wind increases and the v-shaped distribution gradually closes, until it lies around a narrow line aligned along the plume centreline. This is due to the increasing winds reducing the strength of the counter-rotating vortex pair. As a result the standard deviation of the landing position in the $y-$direction, a simple measure of the lateral spread, decreases from 0.55 km in the weakest background-wind simulation to 0.16 km in the strongest background-wind simulation.

Thirdly, the longitudinal spread in the landing position of potential firebrands increases with increasing background wind speed. This is due to the plumes becoming more turbulent and puffy as the background wind speed increases: The potential firebrands that get caught in a puff with a strong enough updraft are transported a long way, whereas potential firebrands that do not get caught in strong enough a puff fall out of the plume much sooner. As a result the standard deviation of the landing position in the $x-$direction, a simple measure of the longitudinal spread, increases from 0.81 km in the weakest background-wind simulation to 3.29 km in the strongest background-wind simulation.

4 Summary and conclusions

We have used a two-stage modelling process to investigate how the dynamics of bushfire plumes can affect long-range spotting and the variation in spread of the landing positions of potential firebrands. Firstly we used the UK Met Office LEM to perform simulations of idealised bushfire plumes under a range of background-wind conditions. Under weak background winds, plumes were intense and the updraft consisted of a coherent counter-rotating vortex pair. Under strong background winds, the plumes were weaker, more bent over and more turbulent, exhibiting pulsing behaviour. Secondly we used a simple Lagrangian particle transport model to explore how the different plume dynamics impacts the trajectories of potential firebrands.

Under the weakest winds the landing positions of potential firebrands exhibited moderate longitudinal spread and large lateral spread. The changes in the plume dynamics that were caused by increasing the background wind speed led to (i) an increase in the mean and maximum spotting distance; (ii) a decrease in the lateral spread of landings positions of potential firebrands; and (iii) an increase in the longitudinal spread of landings positions of potential firebrands. These variations need to be properly accounted for in predictive models of fire spread and systematic studies such as this will form the building blocks of better empirical spotting models.

Acknowledgements

This work was partly supported by the Bushfire Cooperative Research Centre and the Bushfire & Natural Hazards Cooperative Research Centre. We acknowledge the UK Met Office for provision of the LEM code and the assistance of Adrian Hill and Ben Devenish (UKMO) in setting up the simulations.

References

Anthenien, R. A., S. D. Tse, and A. C. Fernandez-Pello, 2006: On the trajectories of embers initially elevated or lofted by small scale ground fire plumes in high winds. *Fire Safety J.*, **41**, 349–363.

Cruz, M. G., A. L. Sullivan, J. S. Gould, N. C. Sims, A. J. Bannister, J. J. Hollis, and R. J. Hurley, 2012: Anatomy of a catastrophic wildfire: The Black Saturday Kilmore East fire in Victoria, Australia. *Forest Ecol. Manag.*, **284**, 269–285.

Ellis, P. F. M., 2010: The effect of the aerodynamic behaviour of flakes of jarrah and karri bark on their potential as firebrands. *J. Roy. Soc. West. Aust.*, **93**, 21–27.

Fawcett, R. J. B., W. Thurston, J. D. Kepert, and K. Tory, 2013: Modelling the fire weather of Black Saturday. *Proceedings of Bushfire CRC & AFAC 2012 Conference Research Forum, 28 August 2012, Perth Australia*, R. P. Thornton and L. J. Wright, Eds., Bushfire CRC, 135–149.

Fric, T. F. and A. Roshko, 1994: Vortical structure in the wake of a transverse jet. *J. Fluid Mech.*, **279**, 1–47.

Gray, M. E. B., J. Petch, S. H. Derbyshire, A. R. Brown, A. P. Lock, H. A. Swann, and P. R. A. Brown, 2001: Version 2.3 of the Met Office large eddy model: Part II. Scientific documentation. Turbulence and Diffusion Note 276, UK Met Office, 49 pp., Exeter, United Kingdom.

Oliveira, L. A., A. G. Lopes, B. R. Baliga, M. Almeida, and D. X. Viegas, 2014: Numerical prediction of size, mass, temperature and trajectory of cylindrical wind-driven firebrands. *Int. J. Wildland Fire*, **23**, 620–630.

Sardoy, N., J.-L. Consalvi, B. Porterie, and A. C. Fernandez-Pello, 2007: Modeling transport and combustion of firebrands from burning trees. *Combust. Flame*, **150**, 151–169.

Thurston, W., K. J. Tory, R. J. B. Fawcett, and J. D. Kepert, 2013: Large-eddy simulations of bushfire plumes in the turbulent atmospheric boundary layer. *MODSIM2013, 20th International Congress on Modelling and Simulation*, J. Piantadosi, R. S. Anderssen, and J. Boland, Eds., Modelling and Simulation Society of Australia and New Zealand, 284–289, ISBN: 978-0-9872143-3-1.